

See discussions, stats, and author profiles for this publication at: <https://www.researchgate.net/publication/231654811>

Nonhydrolytic Route for Synthesis of ZnO and Its Use as a Recyclable Photocatalyst

ARTICLE *in* THE JOURNAL OF PHYSICAL CHEMISTRY C · JANUARY 2010

Impact Factor: 4.77 · DOI: 10.1021/jp910773v

CITATIONS

46

READS

77

2 AUTHORS, INCLUDING:



Deepa Khushalani

Tata Institute of Fundamental Research

41 PUBLICATIONS 1,408 CITATIONS

[SEE PROFILE](#)

Nonhydrolytic Route for Synthesis of ZnO and Its Use as a Recyclable Photocatalyst

Jaykrushna Das[†] and Deepa Khushalani*

Materials Chemistry Group, Department of Chemical Sciences, Tata Institute of Fundamental Research, Mumbai-400 005, India

Received: November 12, 2009; Revised Manuscript Received: December 21, 2009

A simple, convenient and versatile synthetic approach has been demonstrated for large-scale synthesis of zinc glycerolate microcrystals having preferential growth along the (100) axis. Glycerol has been used both as a ligand and as a solvent. This glycerolate precursor has subsequently been converted into the hexagonal phase of zinc oxide (ZnO) with wurtzite structure by calcining in air. A number of techniques, including scanning electron microscopy (SEM), transmission electron microscopy (TEM), X-ray diffraction (XRD), Fourier transform infrared (FTIR) spectroscopy, solid-state ¹³C NMR spectroscopy, and thermogravimetric analysis (TGA) measurements have been used to investigate the morphology, crystallinity, and structure of the products obtained before and after calcination. Furthermore, the room-temperature photoluminescence (PL) of the ZnO nanocrystals has also been investigated along with rhodamine B degradation. The latter has been used as a probe reaction to evaluate the photocatalytic performance of the ZnO nanoparticles for as many as three recycles.

Introduction

Within the group of functional materials, semiconductor metal oxides have received great research attention due to their novel chemical and physical properties that can be exploited for advanced applications.^{1,2} Of these, zinc oxide (ZnO), a representative of II–VI group semiconductor is one of the most attractive and promising materials due to both fundamental research and industrial importance.^{3–6} It exhibits a direct band gap of 3.37 eV at room temperature with a large excitonic binding energy of 60 meV.⁷ This has been extended in its use in a wide variety of applications such as catalysis, support for catalysis, gas-sensor, piezoelectric devices, dye-sensitized solar cells, and photochemical degradation of organic pollutants etc.^{8–13} It has been well established that the functional performances of zinc oxide are contingent on its shape, size, and crystallinity, which in turn are critically dependent on the synthesis conditions. Hence, the control over the size and morphology of ZnO crystals ranging from micrometer to nanometer length scale is a challenge and has become an increasingly active area of research over the past decade. In view of these facts, most of the research in the broad field of materials science is dedicated to the development of different synthetic routes especially in terms of controlling their size, shape and thus architecture.^{14–16}

A variety of physical and chemical methods have been successively employed to fabricate different ZnO nano- and microcrystals in size and morphology. Physical methods like vapor-phase, thermal reduction, pyrolysis, vapor–liquid–solid (VLS) growth, chemical vapor deposition (CVD), metal organic CVD (MOCVD), and molecular beam epitaxy^{17–20} and chemical approaches such as precipitation, sol–gel, and solvothermal processes^{21–26} are very popular among all. However, physical methods always need expensive and sophisticated equipment and complex procedures that restrict further development in

actual application. On the other hand, wet chemical techniques are usually simple, economical, and versatile, which have proved to be very effective for large scale production.^{27–29} However, specifically the aqueous wet chemical method is rather complicated, mainly due to the high reactivity of the metal precursors with water. A simple way to overcome some of the major limitations of aqueous systems is to perform the synthesis procedure in nonhydrolytic solvent. This allows exclusion of water and also in turn the reactivity of metal precursors is decreased, allowing a larger control over the chemical reaction. Although aqueous approaches are very common, it seems that

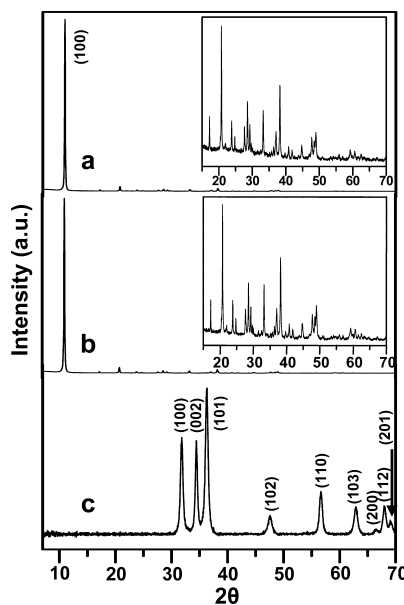


Figure 1. Powder X-ray diffraction patterns of (a) as-synthesized zinc glycerolate complex precursor and (b) the same material after additional grinding for 15 min by a mortar and pestle. (Inset: enlarged view of $2\theta = 15\text{--}70^\circ$). (c) Hexagonal phase of ZnO with wurtzite structure. (Note: the exceptionally strong (100) peak is evident for zinc glycerolate phase as shown in (a) and (b)).

* Corresponding author. E-mail: khushalani@tifr.res.in. Tel: 91-22-22782258. Fax: 91-22-2280 4610/4611.

[†] E-mail: jaykrushna@tifr.res.in.

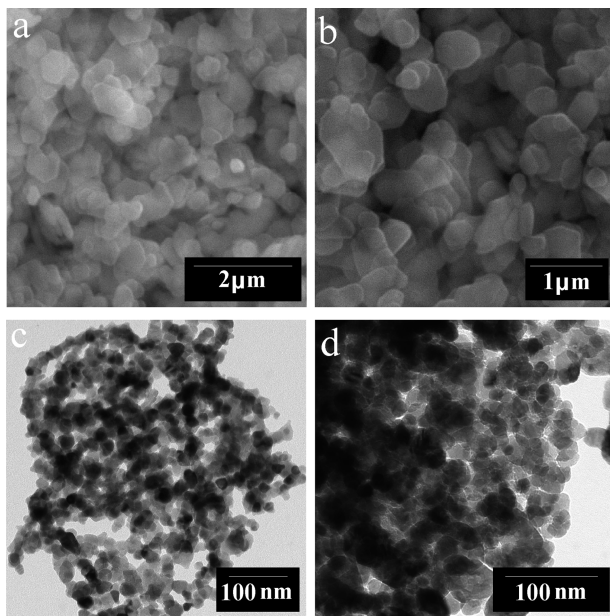


Figure 2. (a), (b) SEM images of zinc glycerolate microcrystal and (c), (d) TEM images of ZnO nanoparticles.

nonaqueous routes are slowly providing a compelling alternative, and this is indicated by the rapidly growing number of papers published following this route for formation of various metal oxides structures.^{30–38}

Moreover, there has been an immense interest in dealing with the environmental pollution issues by designing heterogeneous photocatalysts that eliminate various pollutants in air and in aqueous systems.^{39,40} Among various oxide semiconductors, TiO₂ and ZnO have been recognized as the relevant photocatalysts due to their large band gap, stability, nontoxic nature, cost-effective, and high photosensitivity. Although TiO₂ photocatalysts have been studied more extensively, ZnO is increasingly being used as a suitable substitute due to its similar band gap energy (*ca.* 3.2 eV) and low cost availability. Also, there are some seminal reports in literature describing the higher photocatalytic activity of ZnO than titania.^{41–44} It is worth noting that, although the photocatalytic activities of various nanostructures have been widely established, studies on their renewable photocatalytic behavior are rarely performed.^{13,45–47} One of the main reasons for this drawback is that nanostructures are generally not stable enough and can easily coalesce into a larger entity, leading them to be less readily recoverable for multiple uses.

On the basis of the above reasons, we have developed a new route for synthesis of a unique and novel intermediate precursor, zinc glycerolate in the presence of glycerol. This method is an economic, simple, and a one-step procedure. The synthesis and characterization of the intermediate zinc glycerolate and its consequent conversion to hexagonal phase of ZnO is presented in detail. The photoluminescence (PL) properties of the powders were also investigated. As a demonstration of potential application, the ZnO nanoparticles were assessed for the photodegradation of rhodamine B solution under UV light irradiation under repeated cycles.

Experimental Section

Chemicals and Materials. Reagents employed for the synthesis of ZnO included zinc chloride (98%, ACS, Sigma-Aldrich), glycerol (99%, Merck-India), and sodium hydroxide (97%, SDF Chem.). Rhodamine B was obtained from Sigma-Aldrich. All reagents were used as supplied without further purification.

Synthesis. In a typical synthesis, 1.48 g of a 1:4 molar ratio of zinc chloride (ZnCl₂) and sodium hydroxide (NaOH) were added to 25 mL of glycerol and the mixture was refluxed for 5 h at 190 °C under moderate stirring. After cooling to room temperature (RT), the resultant white precipitate was centrifuged, washed with ethanol to remove excess solvent, and dried at 80 °C for 18 h. This product was calcined from RT to 400 °C at the rate of 5 °C/min and equilibrated for 1 h at 400 °C.

Characterization. X-ray diffraction (XRD) data were collected from powder samples using a PANalytical X'pertpro MPD diffractometer with monochromatic Cu K α radiation ($\lambda = 1.540\text{56}\text{\AA}$). Scanning electron microscopy (SEM) images were taken using JEOL JSM-840. Transmission electron microscopy (TEM) images were captured on a ZEISS, LIBRA-120 machine operated at 120 kV. The Fourier transform infrared (FTIR) spectra of the samples were recorded on a JASCO FT/IR-4100 spectrometer. Thermogravimetric analysis (TGA) measurements were performed on a NETZSCH, STA 409 PC analyzer with a heating rate of 5 °C/min under a flow of N₂-gas. Solid-state cross-polarization/magic angle spinning ¹³C NMR spectrum was taken using a 500 MHz Bruker spectrometer. The PL spectrum was obtained using Spex Fluorolog 1681 spectrometer. Ahead of the data collection, the sample was sonicated in water to obtain visually nonscattering dispersion and the data was recorded immediately.

Measurement of Photocatalytic Activity. The photocatalytic activity of the prepared ZnO was evaluated by the photoassisted decolorization of rhodamine B (RhB) aqueous solution at room

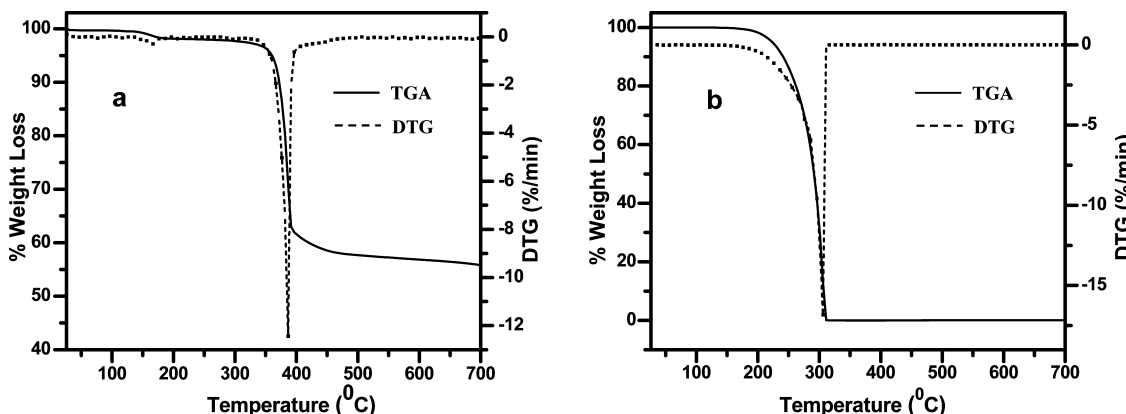


Figure 3. (a) TGA and its corresponding DTG curves of (a) zinc glycerolate and (b) pure glycerol.

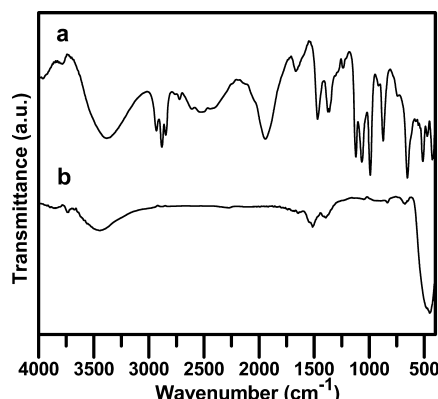


Figure 4. FTIR spectra of (a) zinc glycerolate and (b) zinc glycerolate after calcination to 400 °C.

temperature during irradiation with UV light ($\lambda = 365$ nm). UV light was obtained by four 6W UV lamps. The experimental details were as follows: 0.03 g of the as prepared ZnO powder was dispersed in 30 mL of 1×10^{-5} M RhB aqueous solution in a beaker. Before irradiation, the suspensions were magnetically stirred in the dark for about 6 h to ensure the establishment of adsorption–desorption equilibrium of the dye on the catalyst surface. At given time intervals, 1 mL of reaction mixture was sampled and centrifuged to remove the ZnO nanoparticles. The concentration of RhB was determined by UV–vis spectrophotometer (JASCO V-530). The procedure was performed for three cycles to assess the stability and suitability of ZnO nanoparticles for multiple uses. Blank experiment without addition of ZnO was also carried out as a reference.

Results and Discussion

Powder X-ray diffraction (PXRD) was carried out to investigate the changes of phase structure of the sample before and after calcination. Figure 1a depicts the diffraction profile of the as synthesized sample, and all the peaks were well indexed to the zinc glycerolate phase (JCPDS card No. 00-23-1975). It should be noted that although the position of all the diffraction peaks of zinc glycerolate matches accurately, the relative intensities of the pattern differ with reference to the described JCPDS card. In our case, the (100) peak exhibits an abnormally higher intensity compared to all other peaks, which confirms that the as synthesized zinc glycerolate crystals have preferred orientation along the (100) axis. It should be noted that this was observed even after the crystals were mechanically ground to a finer powder where (100) was still exceptionally intense

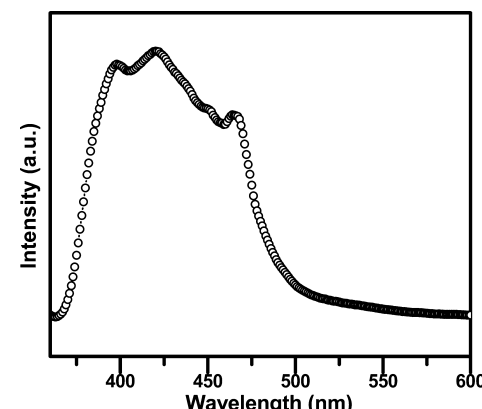


Figure 6. Room temperature PL spectrum of ZnO, obtained after annealing of zinc glycerolate at 400 °C. (The excitation wavelength used is 325 nm.)

(Figure 1b). The structure is known to consist of polymeric sheets constituting zinc ions bridging glycerol, lying parallel to the *bc* plane.⁴⁸ Hence it can be hypothesized that the preferential orientation observed is due to the layered-like structure of zinc glycerolate. Upon subsequent heating of the sample to at least 400 °C, the evolution of the hexagonal phase of wurtzite ZnO (JCPDS File No. 01-089-1397) occurs, as seen in Figure 1c. The morphology of the obtained samples before and after calcination was assessed by electron microscopy, and the representative images are shown in Figure 2. It can be clearly seen that a large number of pseudohexagonal platelike microcrystals of zinc glycerolate were formed, size of ca. 417 ± 92 nm in diameter (Figure 2a,b). Figure 2c,d shows the TEM images of hexagonal phase of ZnO with wurtzite structure after the zinc glycerolate had been calcined in air at 400 °C. These images reveal that the products consist of uniform size spherical nanoparticles of diameter ca. 16.4 ± 3.0 nm. This dramatic change in the structure of the sample can be explained due to the loss of organic ligand, glycerol as well as the phase transformation to ZnO crystallites at higher elevated temperature which is consistent with the XRD analysis as described earlier.

Further, the compositional and structural features of both as synthesized and calcined samples were also assessed using TGA and FTIR spectroscopy. Figure 3 shows a typical TGA and its first-order differential (DTG) curves that were recorded under a flow of N₂ gas at a heating rate 5 °C/min. The TGA curve shows a two-step pattern for weight loss as a function of temperature. The first weight loss, which is very small in amount (~1.8%), in the temperature range 25–200 °C was assigned to

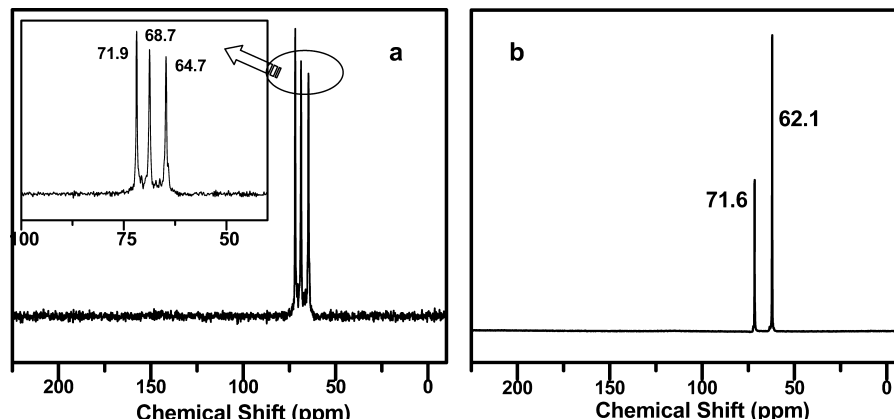


Figure 5. (a) Solid-state CP/MAS ¹³C NMR spectrum of zinc glycerolate and (b) solution spectrum of pure glycerol.

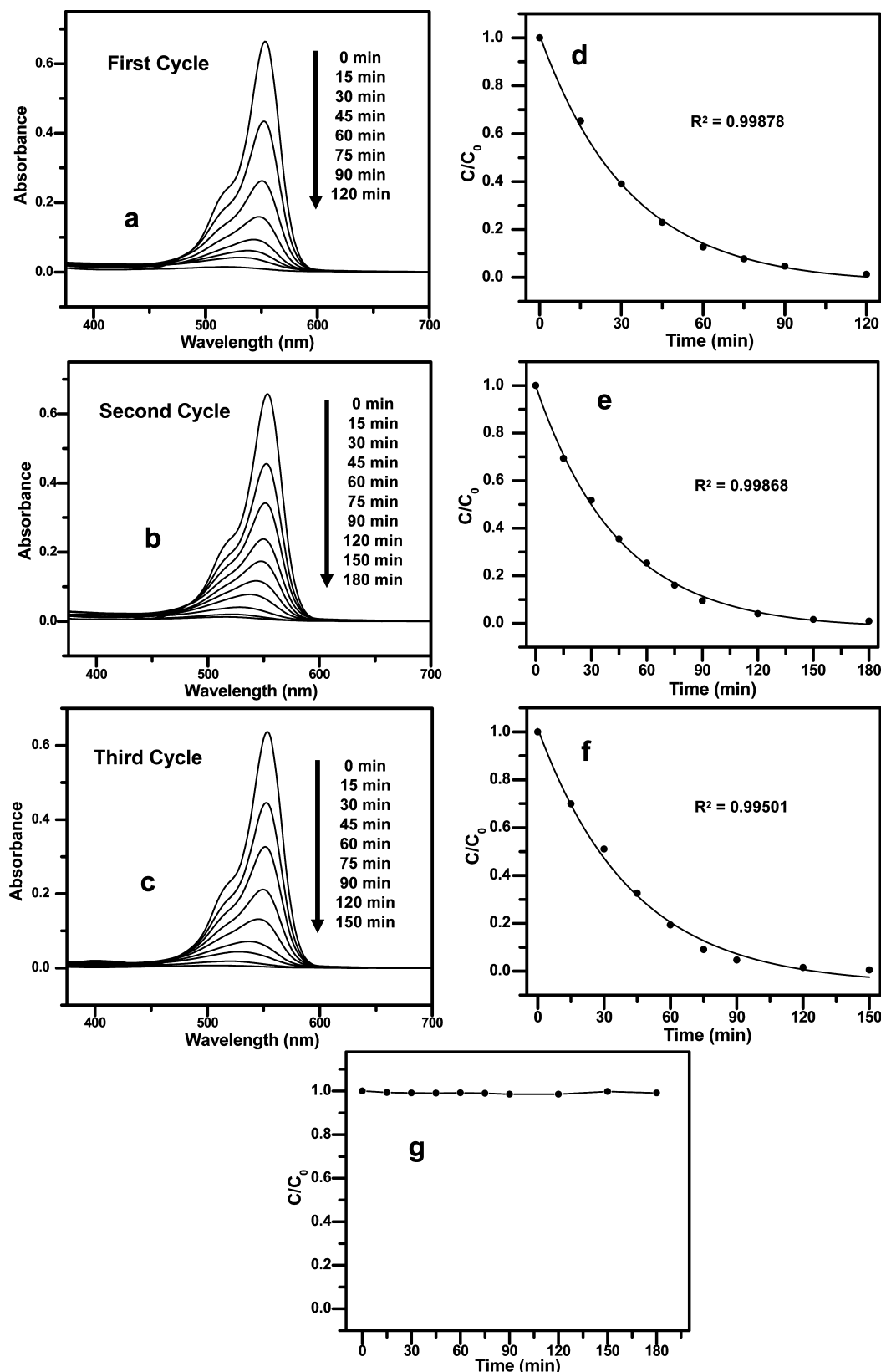


Figure 7. (a)–(c) Time dependent UV–vis spectral changes of RhB in aqueous ZnO suspension under UV-light irradiation for three cycles, (d)–(f) their corresponding photocatalytic degradation curves (C/C_0 vs t), and (g) the concentration changes of only RhB solution without ZnO photocatalyst under exposure to UV-light irradiation.

the loss of physisorbed hydrogen-bonded water, whereas the second one (~42.4% weight loss) in the range 200–700 °C, was attributed to the removal of chemically bonded glycerol moiety (DTG peak at 387 °C), in agreement with the formation of ZnO phase, observed around this temperature by PXRD (see

Figure 1c). The weight loss due to physisorbed water is nominal compared to the second loss, indicating the high degree of purity and superior air stability of the sample unlike other ZnO precursors. It is noteworthy to point out that the pure glycerol gives a sharp and single DTG peak around 307 °C (Figure 3b).

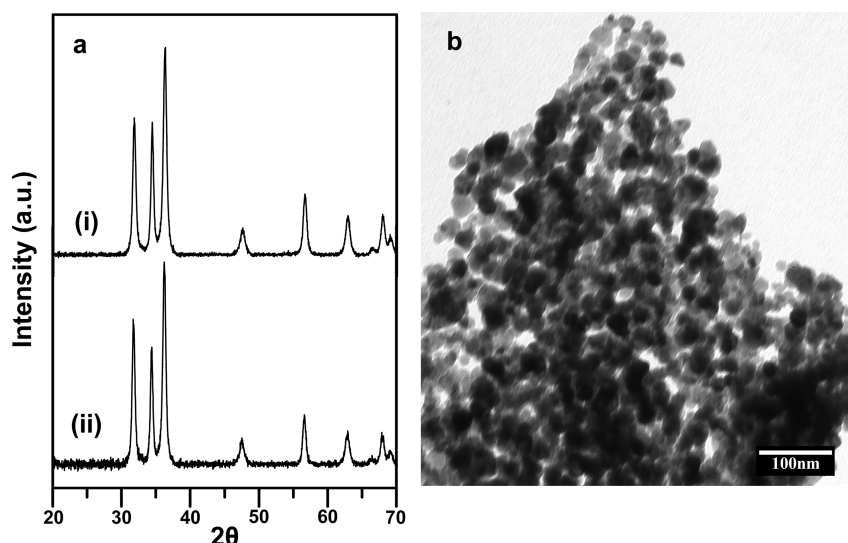


Figure 8. (a) XRD patterns of ZnO (i) before and (ii) after use in the photocatalysis process for three recycles. (b) TEM image of the ZnO nanoparticles after three cycles, which does not show any noticeable change in morphology.

In comparison to pure glycerol, the decomposition temperature of zinc glycerolate is significantly increased, directly suggesting that that glycerol is ligated to zinc center.

Figure 4 shows the FTIR spectra of the as-synthesized zinc glycerolate and after conversion to ZnO phase at 400 °C. The as synthesized zinc glycerolate (Figure 4a) displayed the peaks at *ca.* 1063 and 1124 cm⁻¹, which are assigned to the stretching mode of alcoholic C–O. The bands at 1468 and 1665 cm⁻¹ are due to the O–H bending mode. The peak in the region *ca.* 3200–3500 cm⁻¹ is broad, which could be assigned due to the physically adsorbed water or glycerol O–H stretching mode or hydrogen bonding. The appearance of a new band at 1943 cm⁻¹ confirms the formation of zinc glycerolate phase and can be assigned to ν (C–O) stretching mode where the oxygen atom is involved in an O–H···O hydrogen bond. Apart from these peaks, the peak in between 510–654 cm⁻¹, which is due to the Zn–O stretching mode, indicates the presence of Zn–O bond in the sample. All these peaks are in accordance with the IR bands of zinc glycerolate reported earlier.^{49–51} When zinc glycerolate was calcined for the conversion of hexagonal phase of ZnO, the bands of O–H and C–H were reduced drastically, as depicted in Figure 4b, whereas the Zn–O stretching band was still there, but broadened. In addition, some less intense bands between 750–1025 cm⁻¹ were prevalent which corresponds to the bending and twisting vibrations of ZnOH. The occurrence of moderate peak at *ca.* 3200–3500 cm⁻¹ even after calcination can partly explained the presence of OH on ZnO surface.

Due to the insolubility of the as-synthesized zinc glycerolate powder in most of the common solvents, solid-state CP/MAS ¹³C NMR was performed to gain some insight into the environment of glycerol units and the spectrum is shown in Figure 5. Three distinctly well resolved peaks were observed at 64.7, 68.7, and 71.9 ppm, whereas pure glycerol shows two discrete sharp peaks at 62.1 and 71.6 ppm for the two end C-atoms and the lone middle C-atom, respectively (Figure 5b). As these chemical shifts are observed at lower field (higher ppm value) than the ¹³C-peak of pure glycerol, it is obvious that the C-atoms in the complex are more deshielded and hence this confirms that they are in fact ligated to the positive center of zinc atom through O-atom. In addition, interestingly, glycerol moiety no longer shows degeneracy of the two terminal carbons

and the NMR spectrum clearly shows that they are both in different local electronic environments with respect to pure glycerol.

The room temperature photoluminescence (PL) spectrum of the nanocrystalline ZnO powder was recorded using the excitation wavelength of 325 nm, as displayed in Figure 6. The UV emission at 398 nm was observed, which corresponds to the characteristic near-band-edge emission due to free recombination of exciton, as reported earlier.^{24,37,52} The visible emission band mainly consists of two well-defined peaks: a strong blue band at *ca.* 420 nm and a fairly weak blue-green band at *ca.* 465 nm. In addition to these peaks, a relatively feeble and suppressed tail at the green emission band is present. The origin of blue and blue-green emission is not yet well understood, but the most accepted explanation is possibly due to the surface defects in case of ZnO nanomaterials such as nanoparticles and nanowires, as described in literature.^{53,54} The green emission in ZnO has been associated with oxygen vacancies and vacancy related defects.^{52,55} The weak intensity of the green emission in our sample may be due to the presence of low density of oxygen vacancies during the preparation of ZnO nanoparticles. The higher and stronger UV emission intensity than the vacancies related green band is also an indicative of the high purity with perfect crystallinity of the synthesized ZnO sample.

To demonstrate the potential environmental application, the photocatalytic activity of these ZnO nanoparticles was investigated by evaluating the degradation of rhodamine B (RhB) as a model contaminant. It has been well-established that, upon photoexcitation, the hole that is generated in the valence band has sufficient oxidation potential to initiate aerobic oxidation of many organic compounds. As such, the characteristic absorption peak of RhB at 553 nm was chosen to monitor the photocatalytic degradation process. Figure 7 shows the change of absorption spectra of RhB solution when exposed to UV light at different times in presence of ZnO nanoparticles photocatalyst. The spectrum clearly shows that the absorption peak of RhB drops gradually with an increase of UV exposure time and eventually disappears completely after 120 min, indicating the complete decolorization of RhB aqueous solution during photoassisted reaction. The exponential decay profile of the plot between C/C_0 , (where C_0 and C are the initial and actual

concentration of RhB at time t , respectively) versus time “ t ” (with superb regression coefficient, $R^2 > 0.99$) suggests that the photodecomposition reaction follows first-order rate law and the rate constant was calculated to be 0.031 min^{-1} . The capability of being reusable is one of the most pivotal criteria for an ideal photocatalyst. To further evaluate whether the synthesized ZnO photocatalyst is stable enough for effective photocatalysis, its use as a *recyclable* photocatalyst was further studied for three cycles under the same conditions. The results, given in Figure 7b–f demonstrate that these nanoparticles can indeed serve as highly effective and convenient recyclable photocatalyst. The change in concentration of RhB aqueous solution for multiple steps also fit very well to the exponential decay profile with regression coefficient, $R^2 > 0.99$ and the rate constants were determined to be 0.022 and 0.024 min^{-1} for the second and third cycles, respectively. On the other hand, an additional control experiment demonstrates that the change of concentration of RhB aqueous solution under the exposure to UV light irradiation, without any ZnO photocatalyst, can be ignored (Figure 7g), suggesting that ZnO nanoparticles photocatalyst is necessary for the efficient degradation of RhB aqueous solution. In addition, it should be noted that control experiments performed with bulk ZnO (prepared through normal hydrolytic route) gave a much slower degradation of RhB (rate constant, $k = 0.011 \text{ min}^{-1}$) compared to our as-synthesized ZnO catalyst ($k = 0.031 \text{ min}^{-1}$).

Importantly, the effect on morphology, microstructure, and crystallinity of the photocatalyst after third cycle photodegradation test were monitored using XRD and TEM. The XRD patterns of the catalyst before and after the photoassisted reaction are essentially same, as shown in Figure 8a. Similarly, the TEM examination of the nanoparticles after three cycles did not show any noticeable change in morphology (Figure 8b). These results imply that ZnO nanoparticles were not photocorroded and highly stable even after recycles.

Conclusion

In this study, we have developed a simple process for large scale synthesis of pure and highly crystalline zinc glycerolate crystals unlike reported before where silica matrix and other sacrificial templates were used.^{50,51} The hexagonal phase of ZnO nanoparticles with wurtzite structure was obtained, simply by calcining this zinc glycerolate precursor at 400°C in air. These nanoparticles have been demonstrated to work as effective and recyclable photocatalysts and exhibit excellent photocatalytic activity for the degradation of RhB. XRD and TEM also confirm that the photocatalysts were not photocorroded and stable enough, which does not show any great loss in activity even after many cycles. We believe that this facile nonaqueous route will provide a generic method to prepare other relevant metal oxides, particularly with the possibilities in the environmental applications for the removal of contaminants from wastewater with high activity and stability.

Acknowledgment. We thank cryo-TEM facility of TIFR and Mr. Lalit C. Borde for the help in transmission electron microscopy imaging. We also thank Mr. R. S. Thakur for assistance in the solid-state ^{13}C NMR experiment.

References and Notes

- (1) Kuchibhatla, S.; Karakoti, A. S.; Bera, D.; Seal, S. *Prog. Mater. Sci.* **2007**, *52*, 699–913.
- (2) Wang, Z. L. *Annu. Rev. Phys. Chem.* **2004**, *55*, 159–196.
- (3) Klingshirn, C. *Phys. Status Solidi B* **2007**, *244*, 3027–3073.
- (4) Schmidt-Mende, L.; MacManus-Driscoll, J. L. *Mater. Today* **2007**, *10*, 40–48.
- (5) Chang, P. C.; Lu, J. G. *IEEE Trans. Electron Devices* **2008**, *55*, 2977–2987.
- (6) Ji, S. L.; Ye, C. H. *J. Mater. Sci. Technol.* **2008**, *24*, 457–472.
- (7) Wang, Z. L. *ACS Nano* **2008**, *2*, 1987–1992.
- (8) Goncalves, A. D.; Davolos, M. R.; Masaki, N.; Yanagida, S.; Morandeira, A.; Durrant, J. R.; Freitas, J. N.; Nogueira, A. F. *Dalton Trans.* **2008**, 1487–1491.
- (9) Law, M.; Greene, L. E.; Johnson, J. C.; Saykally, R.; Yang, P. D. *Nat. Mater.* **2005**, *4*, 455–459.
- (10) Pradhan, B.; Batabyal, S. K.; Pal, A. J. *Sol. Energy Mater. Sol. Cells* **2007**, *91*, 769–773.
- (11) Rout, C. S.; Raju, A. R.; Govindaraj, A.; Rao, C. N. R. *J. Nanosci. Nanotechnol.* **2007**, *7*, 1923–1929.
- (12) Wan, Q.; Li, Q. H.; Chen, Y. J.; Wang, T. H.; He, X. L.; Li, J. P.; Lin, C. L. *Appl. Phys. Lett.* **2004**, *84*, 3654–3656.
- (13) Yu, J. G.; Yu, X. X. *Environ. Sci. Technol.* **2008**, *42*, 4902–4907.
- (14) Gao, P. X.; Wang, Z. L. *J. Am. Chem. Soc.* **2003**, *125*, 11299–11305.
- (15) Wang, Z. L. *J. Phys.: Condens. Matter* **2004**, *16*, R829–R858.
- (16) Zheng, Y. H.; Chen, C. Q.; Zhan, Y. Y.; Lin, X. Y.; Zheng, Q.; Wei, K. M.; Zhu, J. F.; Zhu, Y. J. *Inorg. Chem.* **2007**, *46*, 6675–6682.
- (17) Banerjee, D.; Lao, J. Y.; Wang, D. Z.; Huang, J. Y.; Steeves, D.; Kimball, B.; Ren, Z. F. *Nanotechnology* **2004**, *15*, 404–409.
- (18) Lao, J. Y.; Wen, J. G.; Ren, Z. F. *Nano Lett.* **2002**, *2*, 1287–1291.
- (19) Umar, A.; Karunagaran, B.; Suh, E. K.; Hahn, Y. B. *Nanotechnology* **2006**, *17*, 4072–4077.
- (20) Zhang, J.; Yang, Y. D.; Xu, B. L.; Jiang, F. H.; Li, J. P. *J. Cryst. Growth* **2005**, *280*, 509–515.
- (21) Hartlieb, K. J.; Raston, C. L.; Saunders, M. *Chem. Mater.* **2007**, *19*, 5453–5459.
- (22) Wu, X. F.; Bai, H.; Li, C.; Lu, G. W.; Shi, G. Q. *Chem. Commun.* **2006**, 1655–1657.
- (23) Yang, Z.; Liu, Q. H.; Yang, L. *Mater. Res. Bull.* **2007**, *42*, 221–227.
- (24) Zhang, H.; Wu, J. B.; Zhai, C. X.; Du, N.; Ma, X. Y.; Yang, D. *Nanotechnology* **2007**, *18*, 455604–455610.
- (25) Bai, P.; Wu, P. P.; Yan, Z. F.; Zhou, J. K.; Zhao, X. S. *J. Phys. Chem. C* **2007**, *111*, 9729–9733.
- (26) De la Rosa, E.; Sepulveda-Guzman, S.; Rejia-Jayan, B.; Torres, A.; Salas, P.; Elizondo, N.; Yacaman, M. J. *J. Phys. Chem. C* **2007**, *111*, 8489–8495.
- (27) Joo, J.; Kwon, S. G.; Yu, T.; Cho, M.; Lee, J.; Yoon, J.; Hyeon, T. *J. Phys. Chem. B* **2005**, *109*, 15297–15302.
- (28) Chen, Z. T.; Gao, L. *Cryst. Growth Des.* **2008**, *8*, 460–464.
- (29) Wang, L.; Chang, L. X.; Zhao, B.; Yuan, Z. Y.; Shao, G. S.; Zheng, W. J. *Inorg. Chem.* **2008**, *47*, 1443–1452.
- (30) Jiang, X. C.; Wang, Y. L.; Herricks, T.; Xia, Y. N. *J. Mater. Chem.* **2004**, *14*, 695–703.
- (31) Djerdj, I.; Arcon, D.; Jaglicic, Z.; Niederberger, M. *J. Solid State Chem.* **2008**, *181*, 1571–1581.
- (32) Garnweinertner, G.; Niederberger, M. *J. Am. Ceram. Soc.* **2006**, *89*, 1801–1808.
- (33) Niederberger, M. *Acc. Chem. Res.* **2007**, *40*, 793–800.
- (34) Niederberger, M.; Garnweinertner, G. *Chem.—Eur. J.* **2006**, *12*, 7282–7302.
- (35) Niederberger, M.; Garnweinertner, G.; Buha, J.; Polleux, J.; Ba, J. H.; Pinna, N. *J. Sol-Gel Sci. Technol.* **2006**, *40*, 259–266.
- (36) Sui, R. H.; Thangadurai, V.; Berlinguet, C. P. *Chem. Mater.* **2008**, *20*, 7022–7030.
- (37) Das, J.; Evans, I. R.; Khushalani, D. *Inorg. Chem.* **2009**, *48*, 3508–3510.
- (38) Das, J.; Rane, G.; Khushalani, D. *Chem. Lett.* **2009**, *38*, 764–765.
- (39) Hoffmann, M. R.; Martin, S. T.; Choi, W. Y.; Bahnemann, D. W. *Chem. Rev.* **1995**, *95*, 69–96.
- (40) Yu, J. G.; Su, Y. R.; Cheng, B. *Adv. Funct. Mater.* **2007**, *17*, 1984–1990.
- (41) Wan, Q.; Wang, T. H.; Zhao, J. C. *Appl. Phys. Lett.* **2005**, *87*, 083105.
- (42) Sakthivel, S.; Neppolian, B.; Shankar, M. V.; Arabindoo, B.; Palanichamy, M.; Murugesan, V. *Sol. Energy Mater. Sol. Cells* **2003**, *77*, 65–82.
- (43) Khodja, A. A.; Sehili, T.; Pilichowski, J. F.; Boule, P. J. *Photochem. Photobiol. A* **2001**, *141*, 231–239.
- (44) Wang, G.; Chen, D.; Zhang, H.; Zhang, J. Z.; Li, J. H. *J. Phys. Chem. C* **2008**, *112*, 8850–8855.
- (45) Ye, C. H.; Bando, Y.; Shen, G. Z.; Golberg, D. *J. Phys. Chem. B* **2006**, *110*, 15146–15151.
- (46) Kuo, T. J.; Lin, C. N.; Kuo, C. L.; Huang, M. H. *Chem. Mater.* **2007**, *19*, 5143–5147.
- (47) Wang, W. Z.; Zhu, W.; Xu, H. L. *J. Phys. Chem. C* **2008**, *112*, 16754–16758.

- (48) Hambley, T. W.; Snow, M. R. *Aust. J. Chem.* **1983**, *36*, 1249–1253.
- (49) Radoslov., Ew; Raupach, M.; Slade, P. G.; Taylor, R. M. *Aust. J. Chem.* **1970**, *23*, 1963–1971.
- (50) Moleski, R.; Leontidis, E.; Krumeich, F. *J. Colloid Interface Sci.* **2006**, *302*, 246–253.
- (51) Remias, R.; Kukovecz, A.; Daranyi, M.; Kozma, G.; Varga, S.; Konya, Z.; Kiricsi, I. *Eur. J. Inorg. Chem.* **2009**, 3622–3627.
- (52) Zhong, H. M.; Wang, J. B.; Pan, M.; Wang, S. W.; Li, Z. F.; Xu, W. L.; Chen, X. S.; Lu, W. *Mater. Chem. Phys.* **2006**, *97*, 390–393.
- (53) Greene, L. E.; Law, M.; Goldberger, J.; Kim, F.; Johnson, J. C.; Zhang, Y. F.; Saykally, R. J.; Yang, P. D. *Angew. Chem., Int. Ed.* **2003**, *42*, 3031–3034.
- (54) Maensiri, S.; Laokul, P.; Promarak, V. *J. Cryst. Growth* **2006**, *289*, 102–106.
- (55) Cheng, B.; Shi, W. S.; Russell-Tanner, J. M.; Zhang, L.; Samulski, E. T. *Inorg. Chem.* **2006**, *45*, 1208–1214.

JP910773V